



# Ferro-hydrodynamic induced convection flow and heat transfer of nanofluids in a corrugated wall enclosure

Kasra Ayoubi Ayoubloo, Shima Yazdani, Mikhail Sheremet, Obai Younis & Mohammad Ghalambaz

To cite this article: Kasra Ayoubi Ayoubloo, Shima Yazdani, Mikhail Sheremet, Obai Younis & Mohammad Ghalambaz (2023) Ferro-hydrodynamic induced convection flow and heat transfer of nanofluids in a corrugated wall enclosure, Journal of Taibah University for Science, 17:1, 2215675, DOI: [10.1080/16583655.2023.2215675](https://doi.org/10.1080/16583655.2023.2215675)

To link to this article: <https://doi.org/10.1080/16583655.2023.2215675>



© 2023 The Author(s). Published by Informa UK Limited, trading as Taylor & Francis Group



Published online: 09 Jun 2023.



Submit your article to this journal [↗](#)



Article views: 357



View related articles [↗](#)



View Crossmark data [↗](#)

# Ferro-hydrodynamic induced convection flow and heat transfer of nanofluids in a corrugated wall enclosure

Kasra Ayoubi Ayoubloo<sup>a</sup>, Shima Yazdani<sup>b</sup>, Mikhail Sheremet<sup>c</sup>, Obai Younis<sup>d,e</sup> and Mohammad Ghalambaz<sup>id</sup><sup>c</sup>

<sup>a</sup>Department of Mechanical Engineering, Shahid Chamran University of Ahvaz, Ahvaz, Iran; <sup>b</sup>Department of Mechanical Engineering, Quchan University of Technology, Quchan, Iran; <sup>c</sup>Laboratory on Convective Heat and Mass Transfer, Tomsk State University, Tomsk, Russia; <sup>d</sup>Department of Mechanical Engineering, College of Engineering in Wadi Addwasir, Prince Sattam Bin Abdulaziz University, Al-kharj 11942, Saudi Arabia; <sup>e</sup>Department of Mechanical Engineering, Faculty of Engineering, University of Khartoum, Khartoum, Sudan

## ABSTRACT

This study aims to improve heat transfer by utilizing Kelvin forces and inducing magnetic-induced convection in ferro-hydrodynamic convection, in conjunction with nanoparticle migrations. The fundamental equations governing the conservation of mass, momentum, energy, and nanoparticle mass were formulated as partial differential equations. As primary terms, the model incorporated the buoyancy, Lorenz, and Kelvin forces. In this context, temperature variations in the presence of a variable magnetic field generate a temperature-dependent body force. This can induce fluid circulation. Thus, even without gravitational force, magnetic force can stimulate convection heat transfer flows. The study thoroughly examined the impact of magnetic source placement on heat transfer. An increase in  $Ha$  from 0 to 100 reduced the average Nusselt number ( $Nu_{Avg}$ ) by approximately 60% in all cases, regardless of the magnetic source position. However, the magnetic field number ( $Mn_f$ ) and its effect on  $Nu_{Avg}$  are dependent on the magnetic source's position.

## ARTICLE HISTORY

Received 10 February 2023  
Revised 1 May 2023  
Accepted 15 May 2023

## KEYWORDS

Kelvin force; corrugated wall enclosure; two-phase model; ferro-hydrodynamic forces; particle migrations

## 1. Introduction

Heat energy transfer is used in a variety of industrial activities. Natural convection, which does not need external energy, is the most basic kind of convection heat transfer. Most industrial technology, from massive commercial equipment to microchip cooling, relies on heat transfer rate. Improving the heating or cooling of specific industrial processes may be very advantageous since it will save energy and reduce total expenses.

Nanofluids, a novel type of working fluids, have been on exhibit for over 20 years. The ability to retain heat, magnetism, low thermal conductivity, and increased viscosity are all examples of these characteristics. The nanoparticles (NP) in nanofluids are disseminated evenly throughout the base fluid, making it an innovative heat transmission medium [1]. Recent studies have investigated nanofluid convection heat transfer of single/hybrid nanofluid in enclosures [2,3], heat exchangers [4,5], and channels [6]. For instance, Sheremet et al. [7] predicted the natural convection of nanofluids within 2D and 3D porous enclosures. Rates of convection and heat transfer of a nanofluid of alumina and water were investigated by Ibrahim et al. [8] in a 45°-angled square chamber. Based on the results, using nanoparticles enhanced thermal conductivity. The experiment by Paroncini et al. [9] involved the

transfer of heat through natural convection in a cavity having a temperature difference between its sides and an insulated bottom and top.

By using an enclosure with double-sided lids, Sheikholeslami and Chamkha [10] studied the effects of MF variation on the fluid flow properties of nanofluids containing water and  $Fe_3O_4$ . They found that an increase in thermal transfer correlates negatively to the magnetic parameter and positively with the Reynolds and Hartmann numbers. Ghalambaz et al. [11] evaluated the heat and mass transfer of multiple nanofluids within a hexagonal cage subject to a MF. Also, Sami [12] looked at how the presence of an MF created by an element near the collector's intake affected the collector's thermal efficiency. Mokaddes Ali et al. [13] numerically evaluated heat transfer inside a nanofluid water-based container in an external MF. Sathiyamoorthy and Chamkha [14] studied MF's impact on free convection in an enclosure. It was found that the MF and its direction could significantly influence the transfer of heat and flow circulation. Magnetic flows considering Lorentz forces have been investigated in [15–17]. The boundary layer flow and heat transfer of non-Newtonian fluids [18], micro-polar nanofluid [19], and various types of single/hybrid nanoparticles such as graphene oxide [20],  $Fe_2O_3$ –CuO [21],

graphene oxide- $\text{Fe}_3\text{O}_4$  [22], and  $\text{MgO-Ag}$  [23] also were explored.

Huang et al. [24] employed an MF to imitate the convective properties inside a corrugated triangular cavity containing an  $\text{Al}_2\text{O}_3$ -water fluid. Alsabery et al. [25] investigated the free convection of an alumina-water nanofluid in a two-dimensional container with wavy walls that were heated from the bottom without or with a noticeable heater at the bottom. Mahesh et al. [26] studied the chemical reaction on the flow pattern between two stretchy spinning dissipative-viscosity disks and the MF on unsteady hybrid nanobiofluids.

A nanofluid flow can reflect the characteristics of a transient MHD, a ferro-hydrodynamic (FHD) with constant magnetization, or both. The FHD effect results from the interaction between an MF and a magnetized fluid or the Kelvin force. Magnetic nanofluids, also known as ferrofluids, are conventional base liquids seeded with ferromagnetic particles. The magnetic behaviour of ferrofluids in a magnetic field is their most important advantage over other forms of nanofluids [27]. Many researchers studied magnetic nanofluid convection heat transfer mathematically or experimentally. A ferrofluid's thermal conductivity can be improved with chains of magnetic NP bridges, as noted by Liu et al. [28] and Gan Jia Gui et al. [29]. To account for the impacts of both MHD and FHD, Ren et al. [30] created a new technique using multiphase nano-MF in a changeable non-uniform MF.

The investigation of the convection behaviour of nanofluids within cavities has received a great deal of interest lately. Ashorynejad and Shahriari [31] investigated the free convection of a hybrid nanofluid through an enclosure containing a wavy heated wall. Szabo et al.'s [32] numerical analysis of the influence of natural convection on heat transfer in a magnetic nanofluid within a square cavity subjected to a permanent magnet's MF looked at how natural convection changed into thermomagnetic convection. Javed et al. [33] investigated MHD's effects on convection without ferrofluid in a square chamber with obstruction. Bahiraei et al. [34] studied heat transfer along a conduit in which permanent magnets impacted a magnetic nanofluid. Using multiphase mixture models, Mohammadpourfard et al. [35] analysed the impacts of MF on the entropy generation and convection of ferrofluids within cavities. It has been demonstrated that MF applied speeds up convective heat transfer and lowers entropy production. An investigation of the effect of MF on free convection in  $\text{Fe}_3\text{O}_4$ /water ferrofluid has been investigated Abdi et al. [36]. Sheikholeslami et al. [37] looked at the effect of the nanoparticle form on the forced convection of nanofluids under a constant MF. Their findings demonstrated that nanofluid velocity rises with Reynolds and Darcy numbers.

Biswas et al. [38] demonstrated the effect of partially active magnetic fields on the improved thermal performance of a hybrid nanofluid ( $\text{Cu-Al}_2\text{O}_3\text{-H}_2\text{O}$ ) flow in an oblique porous enclosure. The research emphasizes the significance of complex undulating walls and partially active magnetic fields in heat transfer, with a potential improvement of up to 22.16 percent compared to a conventional vertical wall. It also reveals that a partially active magnetic field can control field variables with a smaller reduction in heat transfer (13.97%) than a magnetic field encompassing the entire domain. Mondal et al. [39] examined the thermal-fluid flow of  $\text{Cu/Al}_2\text{O}_3$ -water hybrid nanofluid in a porous enclosure influenced by a horizontal magnetic field using the Brinkman-Forchheimer-Darcy model and a finite volume approach. Findings revealed that heat transfer rate improved with increased frequency, modified Rayleigh number, and porosity but was reduced by nanoparticle addition and higher Darcy and Hartmann numbers. Optimal energy transport was achieved with a bottom-bottom cooler configuration, boosting heat transfer by about 370% compared to uniform heating. This information provides valuable insights for designing efficient thermal devices. Biswas et al. [40] investigated the natural convection flow of oxytactic bacteria subject to a uniform MF in a wavy wall enclosure.

Considering the natural convection heat transfer in a horizontal cylindrical cavity, Chatterjee et al. [41] explored the impact of an inclined magnetic field and discrete wall heating on heat transfer natural convection flows. Considering annuli with partial heating, Chatterjee et al. [42] investigated the magneto-hydrothermal convective dynamics of a nanofluid in a partially cooled porous annuli cavity. Two parts of the outer cylinder were heated while two parts were cooled. An inclined uniform magnetic field was applied to the cylinder and the fluid inside the cavity. Various flow circulation patterns and heat transfer rates could be achieved depending on the arrangements of heated parts. Saha et al. [43] studied free convection in a horizontal cylindrical enclosure with no MF. The right curved wall was heated and left wall was cooled. A circular cavity could lead to a better heat transfer compared to a square cavity.

The topic of thermophoresis and Brownian motion, which lead to an unequal distribution of NPs in the free convection flow within restricted cavities, has recently received much attention. Nanoparticles in nanofluids mostly move through Brownian motion and thermophoresis [44]; nanofluids' free and mixed convection was examined by Garoosi et al. [45] in an adiabatic cage with many sets of heaters and coolers. Their two-phase studies showed that the thermophoresis effects diminish for nanoparticles with high thermal conductivity. A Brownian motion is caused by unequal collisions between molecules, causing suspended NPs to move

chaotically. The concentration gradient of the nanoparticles creates a net mean mass flow as they move about due to Brownian motion. The Brownian motion leads the nanoparticles to scatter equally throughout the liquid. The Brownian motion [46] refers to the random motion of nanoparticles induced by molecules interacting with them in the base fluid.

In conclusion, these studies highlight the significance of magnetic effects, geometry, and heating-cooling arrangements in determining the heat transfer and thermal performance of diverse systems. Whether for energy production, industrial processes, or biomedical applications, they provide valuable insights for designing more efficient thermal devices.

Thermophoresis is caused by a temperature gradient acting through a mixture of particles, which are isotopes or multi-components. Sheremet and Pop [47] computed non-dimensional Lewis and Rayleigh numbers for heat and mass transmission in nanofluids with consideration of the impact of thermophoresis and Brownian motion on NPs embedded in porous media. Soltanipour [48] investigated the effect of MFs non-uniformly affecting an FHD's heat transfer. Brownian, thermophoretic, and magnetophoretic effects are all considered in the two-phase simulation. The results demonstrated that the applied MFs generated a secondary flow with an amplitude several times greater than the input velocity. This research found a sweet spot for the number of magnetic fields that allow maximum heat transmission. Using a spinning disk, Dawar et al. [49] investigated the transfer of heat through 3D MHD nanofluid flows. They also accounted for the Arrhenius activation energy, Brownian motion, and thermophoresis.

Some recent studies examined the impact of a uniform magnetic field on the natural convection flow of nanofluids in horizontal cylindrical enclosures [41, 42]. This is while some of the other literature studies investigated the nanofluids by considering the non-uniform magnetic fields [10,11,50] using single-phase or two-phase approaches. Based on the research review, it is evident that FHD forces depend on the local temperature. Hence, a fluid with a gradient of temperature and non-uniform magnetic fields can produce significant local Kelvin force (FHD), which can induce both convection and flow circulation effects. Convection caused by magnetic flow combined with free convection resulted in convection within an enclosed chamber. Moreover, the movement of heavy NPs caused by the Brownian and thermophoresis effect also induces buoyancy forces, which affect gravity-induced circulations. Thus, the current research is designed to utilize a two-phase model of nanofluids and study the impact of FHD forces and particle migrations on nanofluid convection heat transfer in a corrugated semi-cylindrical chamber for the first time. The impact of MF source location was also addressed.

## 2. Model formulation and description

The present study aims to model and simulate nanofluids' mixed convection heat transfer due to the gravity and FHD effects. Here, Figure 1(a) presents a physical representation of the proposed design. As it is known, the inhomogeneous nanofluid is placed inside a closed cylindrical chamber. Therefore, thermophoresis (movement of nanoparticles due to thermal gradients) and Brownian (random movement of nanoparticles) forces are considered inside the closed chamber [51]. The curved walls on the right and left sides throughout the chamber have a low temperature ( $T_C$ ) and high temperature ( $T_H$ ), respectively. The four sides of the cylinder, with a diameter of  $d$ , have corrugated walls. The angle between every two corrugations is 90 degrees. A conductive wire can be placed in any of these four positions. Thus, the magnetic field with variable strength in space represents the magnetic field induced by a current carrying wire. The magnetic field next to the wire is strong, and its intensity reduces by distance from the wire. The corrugated section of the wall allows a place to fit the wire. The mentioned wire affects the inhomogeneous nanofluid's heat transfer and mass transfer rate at the respective positions. Nanofluid is affected by Kelvin and magnetocaloric forces. Furthermore, the MF can affect the nanofluid's heat transfer and flow rate. Therefore, the Joule-heating and Lorentz forces are also taken into account. The flow is stable and in the laminar regime, while the free convection heat transfer within the chamber will prevail.

Heat transfer and flow can be explained by partial differential equations as follows [11,52,53]:

$$\rho \mathbf{u} \cdot \nabla \mathbf{u} = -\nabla p + \nabla \cdot (\mu \nabla \mathbf{u}) + \mathbf{F} \quad (4)$$

where  $\mathbf{F}$  is the body force, including the buoyancy force ( $F_B$ ), the Lorentz force ( $F_L$ ), and the Kelvin force ( $F_K$ ):

$$\mathbf{F} = \mathbf{F}_B + \mathbf{F}_L + \mathbf{F}_K$$

$$\mathbf{F}_B = \{\rho_p c + (1 - c)[\rho_{bf}(1 - \beta(T - T_C))]\} \mathbf{g}$$

$$\mathbf{F}_L = \mathbf{J} \times \mathbf{B} | \mathbf{J} = \sigma \mathbf{u} \times \mathbf{B} \& \mathbf{B} = \mu_0 \mathbf{H}^*$$

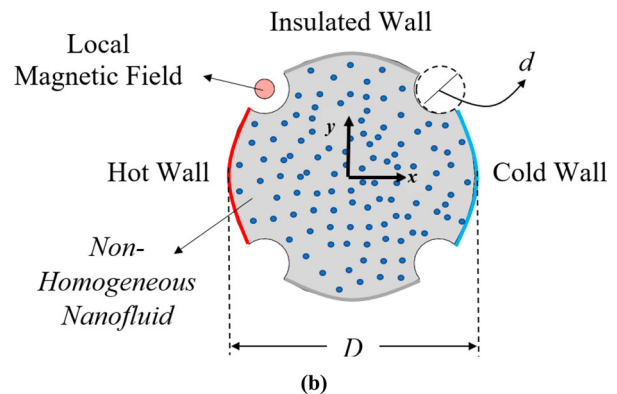


Figure 1. Schematic illustration of the model's physical characteristics.

$$\begin{aligned} \mathbf{F}_K &= \mu_0(\mathbf{M} \cdot \nabla)\mathbf{H}^*|\mathbf{M} = M_x i + M_y j, \quad M_x = M_y \\ &= K' H^* (T_{Cur} - T) \end{aligned} \quad (5)$$

where the buoyancy force includes the change of density due to the migration of nanoparticles.

The energy equation for nanofluid includes the impact of nanoparticles migration ( $Q_F$ ), magnetically induced heat ( $Q_M$ ), and Joule-heating ( $Q_J$ ), which can be explained as [54]:

$$(\rho c_p) \mathbf{u} \cdot \nabla T = \nabla \cdot (\nabla k T) + Q \quad (6)$$

where

$$\begin{aligned} Q &= Q_F + Q_M + Q_J \quad (7a) \\ Q_F &= (\rho c_p)_p \left[ D_B \left( \frac{\partial T}{\partial x} \frac{\partial c}{\partial x} + \frac{\partial c}{\partial y} \frac{\partial T}{\partial y} \right) \right. \\ &\quad \left. + \frac{D_T}{T_c} \left( \left( \frac{\partial T}{\partial x} \right)^2 + \left( \frac{\partial T}{\partial y} \right)^2 \right) \right] \\ Q_M &= \mu_0 T \frac{\partial M}{\partial T} \left( u \frac{\partial H^*}{\partial x} + v \frac{\partial H^*}{\partial y} \right) \\ Q_J &= \sigma (u B_y - v B_x)^2 \quad (7b) \end{aligned}$$

The term with  $D_T$  coefficient represents the thermophoresis force, which tends to move the nanoparticles from hot to cold. The viscous dissipations were ignored since the velocities are very small in a laminar natural convection flow. The nanoparticles migration is governed by the Brownian and thermophoresis forces and is explained as

$$\mathbf{u} \cdot \nabla c = D_B \nabla^2 c + \frac{D_T}{T_c} \nabla^2 T \quad (8)$$

A magnetic point source ( $H^*$ ) is located at the coordinates of  $x_0$  and  $y_0$  at one of the four potential positions, indicated in Figure 1. The  $x$  and  $y$  distance of the source from the origin is  $d$ . The magnetic field due to the source can be explained as [53,55,56]:

$$\begin{aligned} H_x^*(x, y) &= \frac{\delta}{2\pi} \frac{y - y_0}{r}, \\ H_y^*(x, y) &= -\frac{\delta}{2\pi} \frac{x - x_0}{r^2} \end{aligned} \quad (9a)$$

In which

$$H^*(x, y) = (H_x^* + H_y^*)^{\frac{1}{2}} \text{ and } r = ((x - x_0)^2 + (y - y_0)^2)^{\frac{1}{2}} \quad (9b)$$

where  $\delta$  is the MF intensity at the source location. Flow, temperature, and mass transfer boundary conditions associated with the physical schematic (Figure 1) are mathematically described as follows:

on the curved left wall:

$$u = v = 0, T = T_h, D_b \frac{\partial c}{\partial n} + D_t \frac{\partial T}{\partial n} = 0, \quad (10a)$$

on the curved right wall:

$$u = v = 0, T = T_c, D_b \frac{\partial c}{\partial n} + D_t \frac{\partial T}{\partial n} = 0, \quad (10b)$$

on the other walls:

$$u = v = 0, \frac{\partial c}{\partial y} = \frac{\partial T}{\partial y} = 0. \quad (10c)$$

## 2.1. Data reduction

Scaled parameters can reduce boundary conditions and governing equations to a non-dimensional form. Here the following scaled parameters are used:

$$\begin{aligned} P &= \frac{\rho L^2}{\rho \alpha^2}, \theta = \frac{T - T_c}{T_h - T_c}, \phi = \frac{C}{\phi_0}, X = \frac{x}{L}, \\ Y &= \frac{y}{L}, V = \frac{vL}{\alpha}, u = \frac{uL}{\alpha} \quad (11a) \\ H &= \frac{H^*}{H_0^*}, H_X = \frac{H_x^*}{H_0^*}, H_Y = \frac{H_y^*}{H_0^*}, Ra = \frac{g\beta(T_h - T_c)L^3}{\alpha\nu}, \\ Pr &= \frac{\nu}{\alpha}, Ha = L\mu_0 H_0 \sqrt{\frac{\sigma}{\mu}}, Mn_f = \frac{\mu_0 H_0^2 K'(T_h - T_c)L^2}{\mu\alpha} \quad (11b) \end{aligned}$$

$$\begin{aligned} Nr &= \frac{(\rho_p - \rho)\phi_0}{\beta(T_h - T_c)\rho}, Nb = \frac{(\rho c_p)_p D_B \phi_0}{(\rho c_p)\alpha}, \\ Nt &= \frac{(\rho c_p)_p (T_h - T_c) D_T}{(\rho c_p)\alpha T_c}, Le = \frac{\alpha}{D_B} \quad (11c) \end{aligned}$$

in which  $H_{*0} = \delta/(2\pi L)$ . By using the above-scaled parameters, the governing equations can be expressed in the following non-dimensional form:

$$\left( \frac{\partial U}{\partial X} \right) + \left( \frac{\partial V}{\partial Y} \right) = 0 \quad (12)$$

$$\begin{aligned} &\left( U \frac{\partial U}{\partial X} \right) + \left( V \frac{\partial U}{\partial Y} \right) \\ &= - \left( \frac{\partial P}{\partial X} \right) + Pr \left( \frac{\partial^2 U}{\partial X^2} + \frac{\partial^2 U}{\partial Y^2} \right) \\ &\quad - Ha^2 Pr H_Y (U H_Y - V H_X) - Mn_f Pr \theta H \left( \frac{\partial H}{\partial X} \right) \quad (13) \end{aligned}$$

$$\begin{aligned} &\left( U \frac{\partial V}{\partial X} \right) + \left( V \frac{\partial V}{\partial Y} \right) \\ &= - \left( \frac{\partial P}{\partial Y} \right) + Pr \left( \frac{\partial^2 V}{\partial X^2} + \frac{\partial^2 V}{\partial Y^2} \right) + (1 - \phi) Nr Ra Pr \\ &\quad + (1 - \phi\phi_0) Ra Pr \theta \\ &\quad - Ha^2 Pr H_X (V H_X - U H_Y) - Mn_f Pr \theta H \left( \frac{\partial H}{\partial Y} \right) \quad (14) \end{aligned}$$

The term containing  $Ha$  shows the Lorentz force, while  $Mn_f$  denotes the term related to the Kelvin force.



In magnetohydrodynamic (MHD) fluxes, the Lorentz and Kelvin forces are essential. The interaction between an electric current and a magnetic field generates the Lorentz force, which directs charged particles and influences plasma behaviour. In MHD systems, the Kelvin force, a magnetostatic force resulting from varying magnetic field intensity in a conductive fluid, influences fluid flow motion and stability. Both forces, resulting from the interaction of magnetic fields, electric currents, and fluid dynamics, play significant roles in the management of MHD flows. The term containing  $Nr$  shows the change of buoyancy force due to the migration of heavy nanoparticles. Here is the equation of energy for nanofluid:

$$\begin{aligned} & \left( U \frac{\partial \theta}{\partial X} \right) + \left( V \frac{\partial \theta}{\partial Y} \right) \\ &= \left( \frac{\partial^2 \theta}{\partial X^2} + \frac{\partial^2 \theta}{\partial Y^2} \right) \\ &+ Nb \left( \frac{\partial \theta}{\partial X} \frac{\partial \phi}{\partial X} + \frac{\partial \theta}{\partial Y} \frac{\partial \phi}{\partial Y} \right) + Nt \left( \left( \frac{\partial \theta}{\partial X} \right)^2 + \left( \frac{\partial \theta}{\partial Y} \right)^2 \right) \\ &+ EcHa^2 (UH_Y - VH_X)^2 + Mn_f EcH(\varepsilon_1 + \theta) \\ &\left( U \frac{\partial H}{\partial X} + V \frac{\partial H}{\partial Y} \right) \end{aligned} \quad (15)$$

$$\begin{aligned} & Le \left( U \frac{\partial \phi}{\partial X} + V \frac{\partial \phi}{\partial Y} \right) \\ &= \left( \frac{\partial^2 \phi}{\partial X^2} + \frac{\partial^2 \phi}{\partial Y^2} \right) + \frac{Nt}{Nb} \left( \frac{\partial^2 \theta}{\partial X^2} + \frac{\partial^2 \theta}{\partial Y^2} \right) \end{aligned} \quad (16)$$

The boundary conditions are also transformed to the following non-dimensional form:

on the curved left wall ( $\partial\Omega_1$ ):

$$U = V = 0, \theta = 1, Nb \left( \frac{\partial C}{\partial N} \right) + Nt \left( \frac{\partial \theta}{\partial N} \right) = 0, \quad (17a)$$

on the curved right wall ( $\partial\Omega_2$ ):

$$U = V = 0, \theta = 0, Nb \left( \frac{\partial C}{\partial N} \right) + Nt \left( \frac{\partial \theta}{\partial N} \right) = 0, \quad (17b)$$

on the other walls ( $\partial\Omega_3$ ):

$$U = V = 0, \left( \frac{\partial C}{\partial N} \right) = \left( \frac{\partial \theta}{\partial N} \right) = 0. \quad (17c)$$

The enclosure is initially filled by a nanofluid with a non-dimensional concentration of  $\phi = 1$ . Moreover, the following constraints were applied to keep the average concentration of nanoparticles constant:

Over the domain of solution ( $\Omega$ ):

$$\int_{\Omega} \phi / \int_{\Omega} 1 = 1 \quad (17d)$$

A pressure point constrained with a zero relative pressure was to the enclosure's bottom corner for the uniqueness of the pressure distribution and overall solution as:

Over the bottom corner point ( $\Delta$ ):

$$p = 0 \quad (17e)$$

## 2.2. Characteristic parameters

A local Nusselt number is used to analyse heat transfer across heated walls as:

$$Nu_l = - \left. \frac{\partial \theta}{\partial n} \right|_{hot\ wall} \quad (18)$$

In addition, Nusselt's average number was calculated by integrating over the heated wall:

$$Nu_{avg} = \int_S Nu_l dS / \int_S dS \quad (19)$$

where  $S$  refers to the heated wall's nondimensional length.

Furthermore, a nondimensional average velocity was calculated as follows:

$$V_{avg} = \int_A |V| dA / \int_A dA \quad (20)$$

where  $|V|$  is the non-dimensional velocity magnitude computed as  $(U^2 + V^2)^{0.5}$ .

## 3. Numerical model and code verification

### 3.1. Numerical method

The finite element method (FEM) [57,58] was invoked to integrate the equations of Equations (12)–(16), in conjunction with Equation (17) (boundary conditions). According to the FEM, equations were converted into a weak form and then integrated over discretized elements. Quadratic shape functions were adopted as the weights. Each of the field variables  $U$ ,  $V$ ,  $P$ ,  $\theta$ , and  $C$  was introduced using a basis function  $\xi$  as:

$$\begin{aligned} U &\approx \sum_{i=1}^N U_i \xi(X, Y), V \approx \sum_{i=1}^N V_i \xi(X, Y), \\ P &\approx \sum_{i=1}^N P_i \xi(X, Y), \\ \theta &\approx \sum_{i=1}^N \theta_i \xi(X, Y), \\ \phi &\approx \sum_{i=1}^N \phi_i \xi(X, Y), \end{aligned} \quad (21)$$

The basic form of field variables, Equation (21), is plugged into weak forms of the governing equations in order to obtain the discretized algebraic equations as follows

The continuity equation:

$$R_1^1 : \left\{ \int_{\Omega} \left( \left( \frac{\partial \xi_i(X, Y)}{\partial Y} \right) \left( \sum_{m=1}^N V_m \left( \frac{\partial \xi_m(X, Y)}{\partial Y} \right) \right) \right) + \left( \frac{\partial \xi_i(X, Y)}{\partial X} \right) \left( \sum_{m=1}^N U_m \left( \frac{\partial \xi_m(X, Y)}{\partial X} \right) \right) \right\} \xi_i(X, Y) = 0 \quad (22a)$$

X-Momentum:

$$R_1^2 : - \int_{\Omega} \left( \left( \frac{\partial \xi_i(X, Y)}{\partial X} \right) \left( - \Pr \left( \sum_{m=1}^N U_m \left( \frac{\partial \xi_m(X, Y)}{\partial X} \right) \right) + \left( \sum_{m=1}^N P_m \xi_m(X, Y) \right) \right) + \left( \frac{\partial \xi_i(X, Y)}{\partial Y} \right) \times \left( \Pr \sum_{m=1}^N U_m \left( \frac{\partial \xi_m(X, Y)}{\partial Y} \right) \right) - \int_{\Omega} \left( \left( \left( \sum_{m=1}^N U_m \left( \frac{\partial \xi_m(X, Y)}{\partial X} \right) \right) \times \left( \sum_{m=1}^N U_m \xi_m(X, Y) \right) \right) + \left( \left( \sum_{m=1}^N U_m \left( \frac{\partial \xi_m(X, Y)}{\partial Y} \right) \right) \times \left( \sum_{m=1}^N V_m \xi_m(X, Y) \right) \right) \right) \xi_i(X, Y) - Ha^2 \Pr \int_{\Omega} \left( \left( H_Y(X, Y) \times \sum_{m=1}^N U_m \xi_m(X, Y) \right) \times - \left( H_X(X, Y) \times \sum_{m=1}^N V_m \xi_m(X, Y) \right) \right) \xi_i(X, Y) - Mn_f \Pr \int_{\Omega} H(X, Y) \times \left( \frac{\partial H(X, Y)}{\partial X} \right) \times \left( \sum_{m=1}^N \theta_m \xi_m(X, Y) \right) \xi_i(X, Y) = 0 \quad (22b)$$

Y-Momentum:

$$R_1^3 : - \int_{\Omega} \left( \left( \frac{\partial \xi_i(X, Y)}{\partial X} \right) \left( \Pr \sum_{m=1}^N V_m \left( \frac{\partial \xi_m(X, Y)}{\partial X} \right) \right) + \left( \frac{\partial \xi_i(X, Y)}{\partial Y} \right) \times \left( - \Pr \sum_{m=1}^N V_m \left( \frac{\partial \xi_m(X, Y)}{\partial Y} \right) + \sum_{m=1}^N P_m \xi_m(X, Y) \right) - \int_{\Omega} \left( \left( \sum_{m=1}^N U_m \xi_m(X, Y) \times \sum_{m=1}^N V_m \left( \frac{\partial \xi_m(X, Y)}{\partial X} \right) \right) + \left( \sum_{m=1}^N V_m \xi_m(X, Y) \times \sum_{m=1}^N V_m \left( \frac{\partial \xi_m(X, Y)}{\partial Y} \right) \right) \right) \xi_i(X, Y)$$

$$\times \xi_i(X, Y) + NrRa \Pr \int_{\Omega} \left( 1 - \sum_{m=1}^N \phi_m \xi_m(X, Y) \right) \xi_i(X, Y) + Ra \Pr \int_{\Omega} \sum_{m=1}^N \theta_m \xi_m(X, Y) \times \left( 1 - \phi_0 \sum_{m=1}^N \phi_m \xi_m(X, Y) \right) \xi_i(X, Y) - Ha^2 \Pr \int_{\Omega} \left( \left( H_X(X, Y) \times \sum_{m=1}^N V_m \xi_m(X, Y) \right) - \left( H_Y(X, Y) \times \sum_{m=1}^N U_m \xi_m(X, Y) \right) \right) \xi_i(X, Y) - Mn_f \Pr \int_{\Omega} H(X, Y) \times \frac{\partial H(X, Y)}{\partial Y} \left( \sum_{m=1}^N \theta_m \xi_m(X, Y) \right) \xi_i(X, Y) = 0 \quad (22c)$$

Along a pressure point constraint as  $-\int_{\Lambda}$

$$\left( \sum_{m=1}^N P_m \xi_m(X, Y) \right) \xi_i(X, Y) = 0.$$

For the heat equation:

$$R_1^4 : - \int_{\Omega} \left( \left( \left( \frac{\partial \xi_i(X, Y)}{\partial Y} \right) \sum_{m=1}^N \theta_m \frac{\partial \xi_m(X, Y)}{\partial Y} \right) + \left( \frac{\partial \xi_i(X, Y)}{\partial X} \sum_{m=1}^N \theta_m \left( \frac{\partial \xi_m(X, Y)}{\partial X} \right) \right) - \int_{\Omega} \left( \left( \sum_{m=1}^N U_m \xi_m(X, Y) \times \sum_{m=1}^N \theta_m \left( \frac{\partial \xi_m(X, Y)}{\partial X} \right) \right) + \left( \sum_{m=1}^N V_m \xi_m(X, Y) \sum_{m=1}^N \theta_m \left( \frac{\partial \xi_m(X, Y)}{\partial Y} \right) \right) \right) \xi_i(X, Y) + Nb \int_{\Omega} \left( \left( \sum_{m=1}^N \phi_m \left( \frac{\partial \xi_m(X, Y)}{\partial X} \right) \times \sum_{m=1}^N \theta_m \left( \frac{\partial \xi_m(X, Y)}{\partial X} \right) \right) + \left( \sum_{m=1}^N \phi_m \left( \frac{\partial \xi_m(X, Y)}{\partial Y} \right) \times \sum_{m=1}^N \theta_m \left( \frac{\partial \xi_m(X, Y)}{\partial Y} \right) \right) \right) \xi_i(X, Y) + Nt \int_{\Omega} \left( \left( \sum_{m=1}^N \theta_m \left( \frac{\partial \xi_m(X, Y)}{\partial X} \right) \times \sum_{m=1}^N \theta_m \left( \frac{\partial \xi_m(X, Y)}{\partial X} \right) \right) + \left( \sum_{m=1}^N \theta_m \left( \frac{\partial \xi_m(X, Y)}{\partial Y} \right) \times \sum_{m=1}^N \theta_m \left( \frac{\partial \xi_m(X, Y)}{\partial Y} \right) \right) \right) \xi_i(X, Y)$$

$$\begin{aligned}
& + Ec \times Ha^2 \int_{\Omega} \left( -H_X(X, Y) \times \sum_{m=1}^N V_m \xi_m(X, Y) \right. \\
& \times \left. + H_Y(X, Y) \times \sum_{m=1}^N U_m \xi_m(X, Y) \right) \xi_i(X, Y) \\
& + Ec \times Mn_f \int_{\Omega} \left( H(X, Y)(\varepsilon_1 + \theta) \left[ \left( \frac{\partial H(X, Y)}{\partial Y} \right) \right. \right. \\
& \times \sum_{m=1}^N V_m \xi_m(X, Y) \left. + \left( \frac{\partial H(X, Y)}{\partial X} \right) \right. \\
& \times \left. \left. \sum_{m=1}^N U_m \xi_m(X, Y) \right] \right) \xi_i(X, Y) \\
& = - \int_{\partial\Omega} \left( \xi_i(X, Y) \lambda_1 + \lambda_{1,i}(X, Y) \left( \sum_{m=1}^N \theta_m \xi_m(X, Y) - 1 \right) \right) \\
& + \left( \xi_i(X, Y) \lambda_2 + \lambda_{2,i}(X, Y) \sum_{m=1}^N \theta_m \xi_m(X, Y) \right) \quad (22d)
\end{aligned}$$

where  $\lambda_1$  and  $\lambda_2$  represent the unknown heat fluxes to be determined at the isotherm boundaries (cold and hot walls) of domains  $\partial\Omega$ .

For the concentration of nanoparticles:

$$\begin{aligned}
R_i^5 : & - \int_{\Omega} \left( \left( \left( \frac{\partial \xi_i(X, Y)}{\partial Y} \right) \sum_{m=1}^N \phi_m \left( \frac{\partial \xi_m(X, Y)}{\partial Y} \right) \right. \right. \\
& + \left( \left( \frac{\partial \xi_i(X, Y)}{\partial X} \right) \sum_{m=1}^N \phi_m \left( \frac{\partial \xi_m(X, Y)}{\partial X} \right) \right) \left. \right) \\
& + Le \times \int_{\Omega} \left( \left( \sum_{m=1}^N \phi_m \left( \frac{\partial \xi_m(X, Y)}{\partial X} \right) \right. \right. \\
& \times \left( \sum_{m=1}^N U_m \xi_m(X, Y) \right) \left. + \left( \sum_{m=1}^N \phi_m \left( \frac{\partial \xi_m(X, Y)}{\partial Y} \right) \right) \right. \\
& \times \left( \sum_{m=1}^N V_m \xi_m(X, Y) \right) \left. \right) \xi_i(X, Y) \\
& + \frac{Nt}{Nb} \int_{\Omega} \left( \left( \sum_{m=1}^N \theta_m \frac{\partial \xi_m(X, Y)}{\partial X} \right) \times \left( \frac{\partial \xi_i(X, Y)}{\partial X} \right) \right. \\
& + \left. \left( \sum_{m=1}^N \theta_m \frac{\partial \xi_m(X, Y)}{\partial Y} \right) \times \left( \frac{\partial \xi_i(X, Y)}{\partial Y} \right) \right) = 0 \quad (22e)
\end{aligned}$$

along with the following constrain.

$$- \int_{\Omega} \left[ \int_{\Omega} \left( 1 - \sum_{m=1}^N \phi_m \xi_m(X, Y) \right) / \int_{\Omega} 1 \right] \xi_i(X, Y) \quad \text{over}$$
 the whole domain of the solution.

The momentum and heat equations were subject to second-order discretization. The residual equations were then addressed utilizing the Newton method, employing a fully coupled scheme to determine the unknown fields across the solution domain. To ensure solution accuracy within a relative error of 10E-4, an automatic step control was utilized. Subsequent sections discuss grid validation and method verification. More details about the numerical method can be found in [59–61].

### 3.2. Grid testing

Simulating heat transfer in an enclosure using several mesh sizes was investigated to determine the effect of mesh size on calculation accuracy. The computations were repeated for a case with  $Ra = 5 \times 10^5$ ,  $\varphi = 0.05$ ,  $Ha = 50$ ,  $Mn_f = 3000$ , and  $Pr = 7$ . Five meshes with 7126; 15,616; 33,278; 51,702; and 88,396 elements were utilized. For a more accurate representation of the velocity, temperature, and mass transfer gradients, the mesh density is higher near the walls. The mesh is coarse and far from the walls to reduce computational costs. Table 1 reports the results of calculating the average Nusselt number for the selected mesh sizes. As seen,

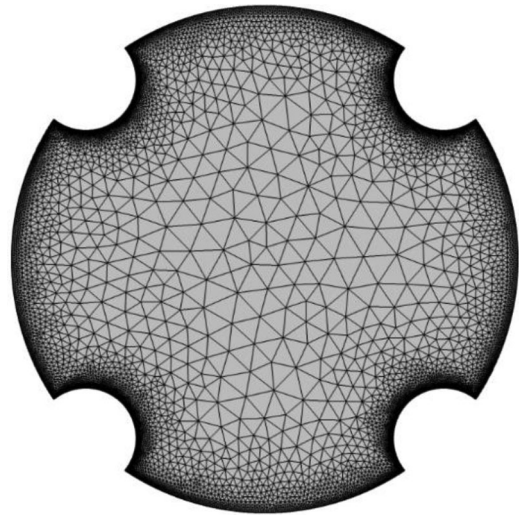


**Figure 2.** The mesh pattern in the geometry. As far as velocity, temperature, and mass gradients are concerned, the mesh is fine next to the walls.

**Table 1.** Comparison of  $Nu_{Avg}$  for a variety of grid sizes at  $Ra = 5 \times 10^5$ ,  $\varphi = 0.05$ ,  $Ha = 50$ ,  $Mn_f = 3000$  and  $Pr = 7$ .

Number of elements (Domain Elements)	7126	15,616	<b>33,278</b>	51,702	88,396
$Nu_{Avg}$	3.45123	2.86870	<b>3.30757</b>	3.31246	3.30771
error (%)	4.3	–13.27	–0.0042	0.1436	–

Note: the bold column was selected for computations of the results section.

$$error(\%) = \left| \frac{Nu - Nu_{fine}}{Nu_{fine}} \right| \times 100, \text{ where } Nu_{fine} = 3.30771.$$



a mesh with 33,278 elements provides a tiny error. Thus, this mesh size was adopted for the computations. Figure 2 shows a view of the adopted mesh.

### 3.3. Model verification

A comparison between the present paper's findings and Sathiyamoorthy and Chamkha's results [14] was performed in Figure 3. In addition, the isotherms obtained in this study were compared with those obtained by Paroncini et al. [9] in Figure 4. Both cases show excellent agreement with the literature studies.

## 4. Results and discussion

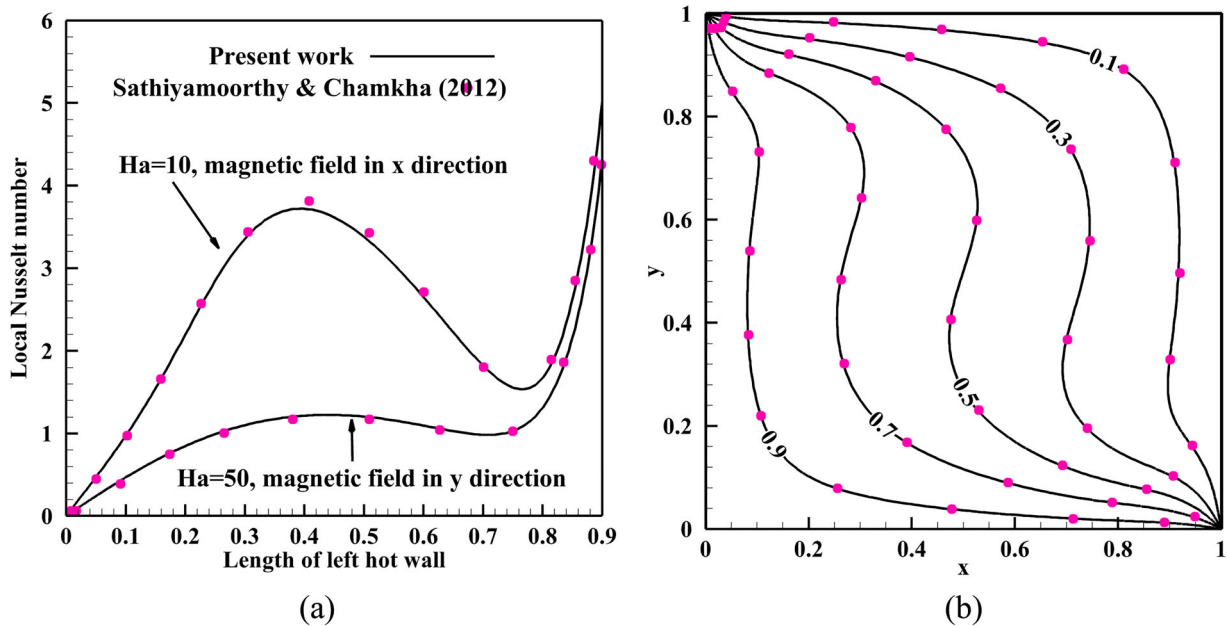
The range of governing variables is  $M_{nf} = 0-4 \times 10^4$ , while other parameters are considered to be constant

so that  $Ra = 5 \times 10^5$ ,  $\varphi = 5\%$ , and  $Pr = 7$ . The nanofluids typically have a low volume fraction of nanoparticles [62, 63]. The volume concentration of nanofluids up to 5% for the two-phase Buongiorno model has been suggested by Buongiorno [51]. Hartmann number is adopted in the range  $Ha = 0-100$ , which agrees with the 0–100 [64, 65] and 30 [66] adopted in the literature. It should be noted that reaching large  $Ha$  numbers

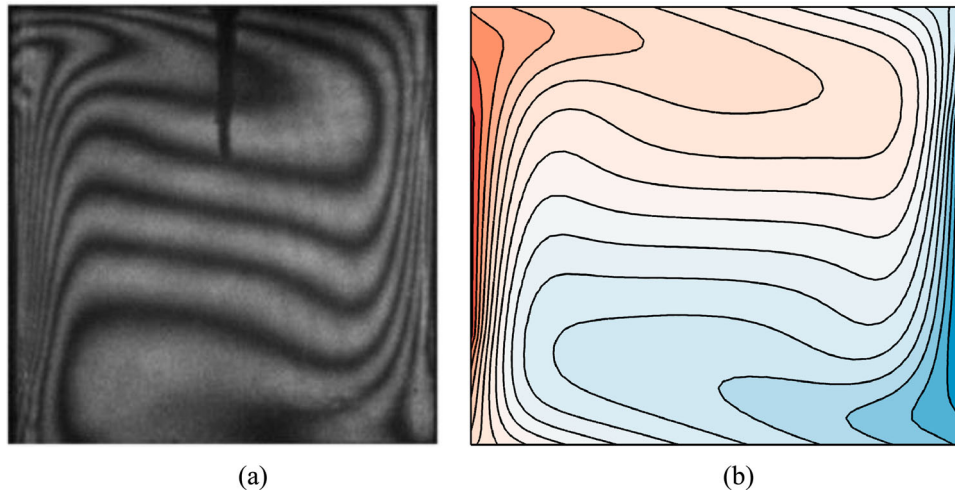
**Table 2.** Magnetic source changes in the situation.

	Cases	$d_1^*$	$d_2^*$	Placement of the local magnetic field
<b>SIGN</b>	<b>I</b>	+	+	<b>LB</b>
	<b>II</b>	+	–	<b>RB</b>
	<b>III</b>	–	–	<b>RT</b>
	<b>IV</b>	–	+	<b>LT</b>

Note: T = Top, B = Bottom, R = Right, L = Left.

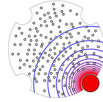


**Figure 3.** Comparison between the present numerical results and those of Sathiyamoorthy and Chamkha [14] for enclosure heat transfer with MHD effects. (a) The local average Nusselt number for two cases of the MF in x and y directions. (b) The isotherms when the magnetic field is applied along the y direction and Hartmann number,  $Ha = 50$ .



**Figure 4.** Comparison of the experimental measurements made by Paroncini et al. [9] with the present calculation when  $Ra = 2.28 \times 10^5$  (with permission from Elsevier).

**Table 3.** Average velocity and Nusselt number at the various locality of a magnetic source and when  $Ha = 100$ ,  $M_{nf} = 30,000$ ,  $Ra = 5 \times 10^5$ ,  $Pr = 7$ , and  $\varphi = 5\%$ .

Case	Position of the local magnetic field	$Nu$	$V_{avg}$
I		2.2282	11.0148
II		<b>2.4566</b>	<b>11.1648</b>
III		1.9376	9.3596
IV		1.6906	17.4776

is difficult and requires strong magnetic fields. Thus, a fair value of  $Ha$  number much smaller than 100 should be adopted. However, since the present study is a non-dimensional investigation focusing on the trend of the physical results, a large value of  $Ha$  was adopted to better show the physical trends.

Table 2 shows that if  $d_1^*$  and  $d_2^*$  are changed to a different sign, the local magnetic source formed by the conducting wire can be moved to a different situation, as shown.

The positioning of the conductive magnetic source can vary considerably, as detailed in Table 3. The location of this magnetic source can exert a substantial influence on the heat and mass transfer rate within a homogeneous nanofluid. Given the likelihood of non-dimensional parameters being governed by multiple variables, the Nusselt number, along with the velocity of

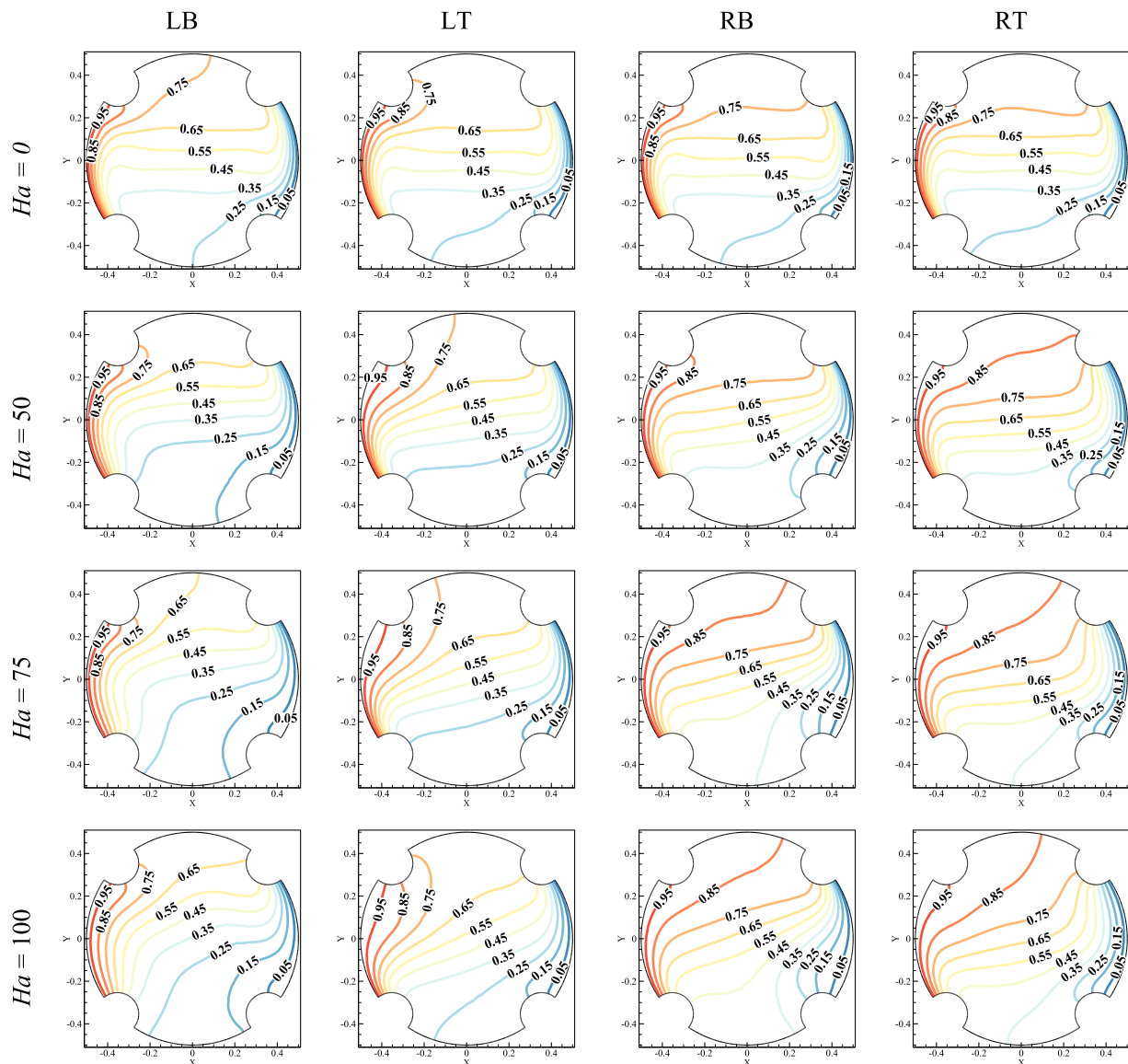


**Figure 5.** Isotherm lines change on  $Ha$  and  $\delta$  when  $Ra = 5 \times 10^5$ ,  $\varphi = 5\%$ ,  $Pr = 7$  and  $M_{nf} = 30,000$ .

the nanofluid, will be provided for these variables. The research findings indicate that the maximum rates of heat and mass transfer are achieved in situation II, while the minimum rates are observed in situation IV. Conversely, the peak and trough average velocity values are recorded in situations IV and III, respectively.

It's critical to note that an increase in the velocity of the nanofluid within the enclosure doesn't necessarily result in a corresponding enhancement of heat and mass transfer mechanisms. This observation adds a layer of complexity to the understanding of fluid dynamics and heat transfer in such systems and invites further investigation.

As seen in Figure 5, the isotherms of the MF are affected by the  $Ha$  and the location of the magnetic source. At  $Ha = 0$ , the Kelvin force is the only force arising from the magnetic field, and it is linked to the variable nature of the applied magnetic field. Since the

intensity of the applied magnetic source changes by the distance from the source, it induces a Kelvin body force. This force is a function of the magnetic field and its gradient. Clearly, the Kelvin force can notably impact the isotherms next to the walls where the magnetic field and its gradients are strong. On the other hand, changing the locality of the magnetic source can increase the flow strength when  $Ha = 0$ , while the non-zero values of the Hartmann number reduce the velocity. It is evident from the figure that the increase in the flow strength is the highest for RB.

Furthermore, when  $Ha \neq 0$ , the Lorentz force is also applied to the fluid domain. Lorentz's resistance force is more potent than Kelvin's. This force is always perpendicular to the nanofluid's velocity and the magnetic field's direction. Therefore, increasing the  $Ha$  decreases the nanofluid velocity. Additionally, an increase in  $Ha$  thickens the thermal boundary layers.

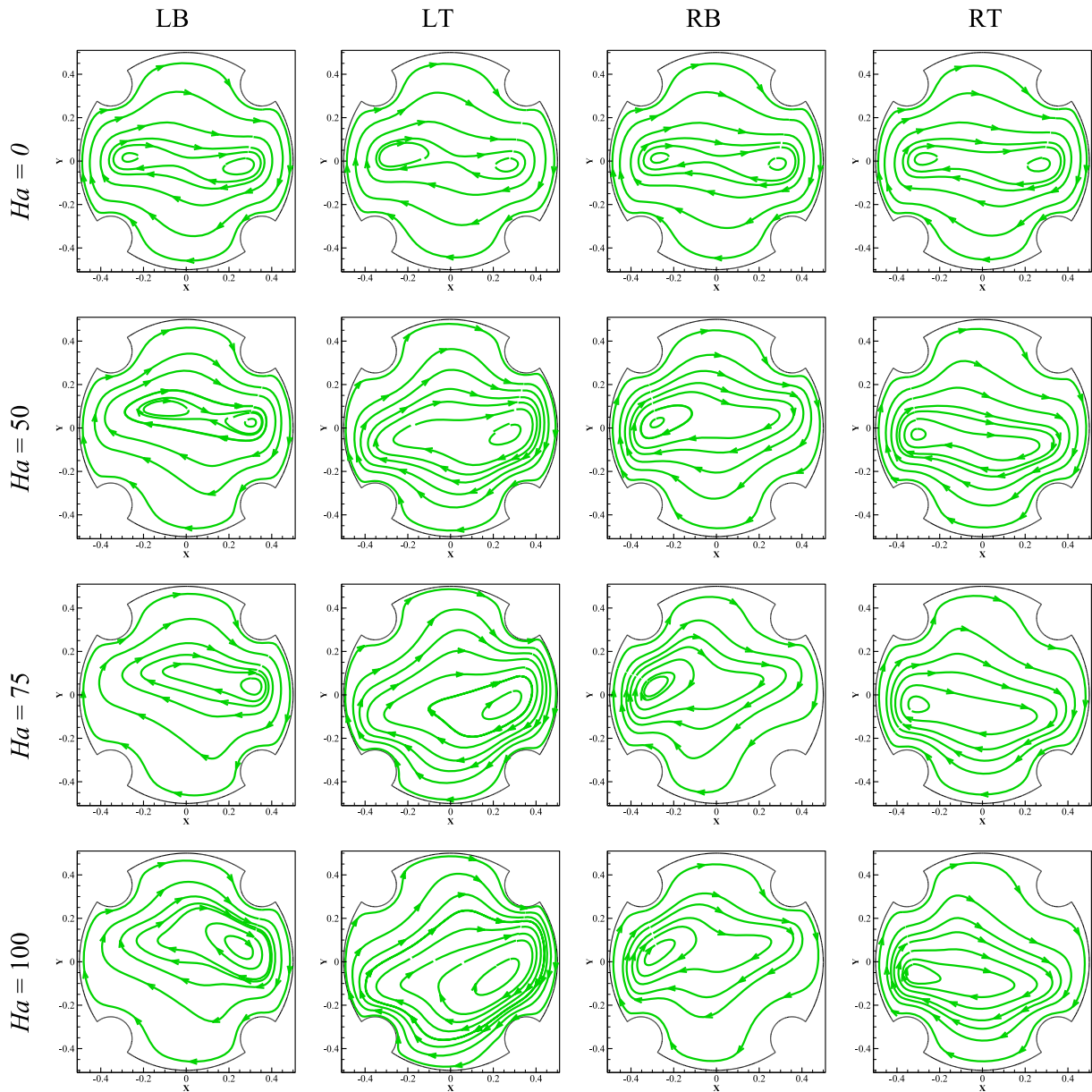


**Figure 6.** Streamlines change on  $Ha$  and  $\delta$  when  $Ra = 5 \times 10^5$ ,  $\varphi = 5\%$ ,  $Pr = 7$  and  $M_{nf} = 30,000$

In Figure 6, the streamlines delineate the trajectory of the nanofluid within the enclosure under different Hartmann numbers. The data in this figure underscores the significant effect of the magnetic source on the streamlines in its immediate vicinity. The magnetic source exerts a potent resistive force on the nearby nanofluid, leading to a localized decrease in the fluid's velocity. As a result, a distinct separation is observed in the streamlines near the magnetic source. As the distance from the magnetic source increases, the nanofluid's velocity picks up to offset the decreased flow velocity near the magnetic source, thus ensuring the continuity of the overall flow circulation within the enclosure.

Figure 7 displays the local concentration of nanoparticles inside the enclosure for various values of Hartmann number. The thermophoresis force tends to move nanoparticles away from the hot wall. The Brownian motion uniformizes the nanoparticles by moving them

from a high concentration area to a low concentration area. The Lorentz and Kelvin forces can indirectly impact the nanoparticle's distribution through velocity and temperature fields. As seen, the presence of a magnetic source induces non-symmetric effects for nanoparticle concentrations. The increase of  $Ha$  number boosts the impact of magnetic source location on the concentration patterns. This is because a large  $Ha$  more intensively impacts the flow and temperature fields and, consequently, the nanoparticle distributions.

Figure 8 illustrates how the isotherms depend on the location of the magnetic source and  $M_{nf}$ .  $M_{nf}$  controls the strength of Kelvin forces, and an increase in  $M_{nf}$  parameter increases the strength of Kelvin forces. Attention to the cases  $M_{nf} = 0$  and  $M_{nf} = 1 \times 10^4$  shows that the presence of magnetic source notably impacts the local temperature distribution. For example, Kelvin

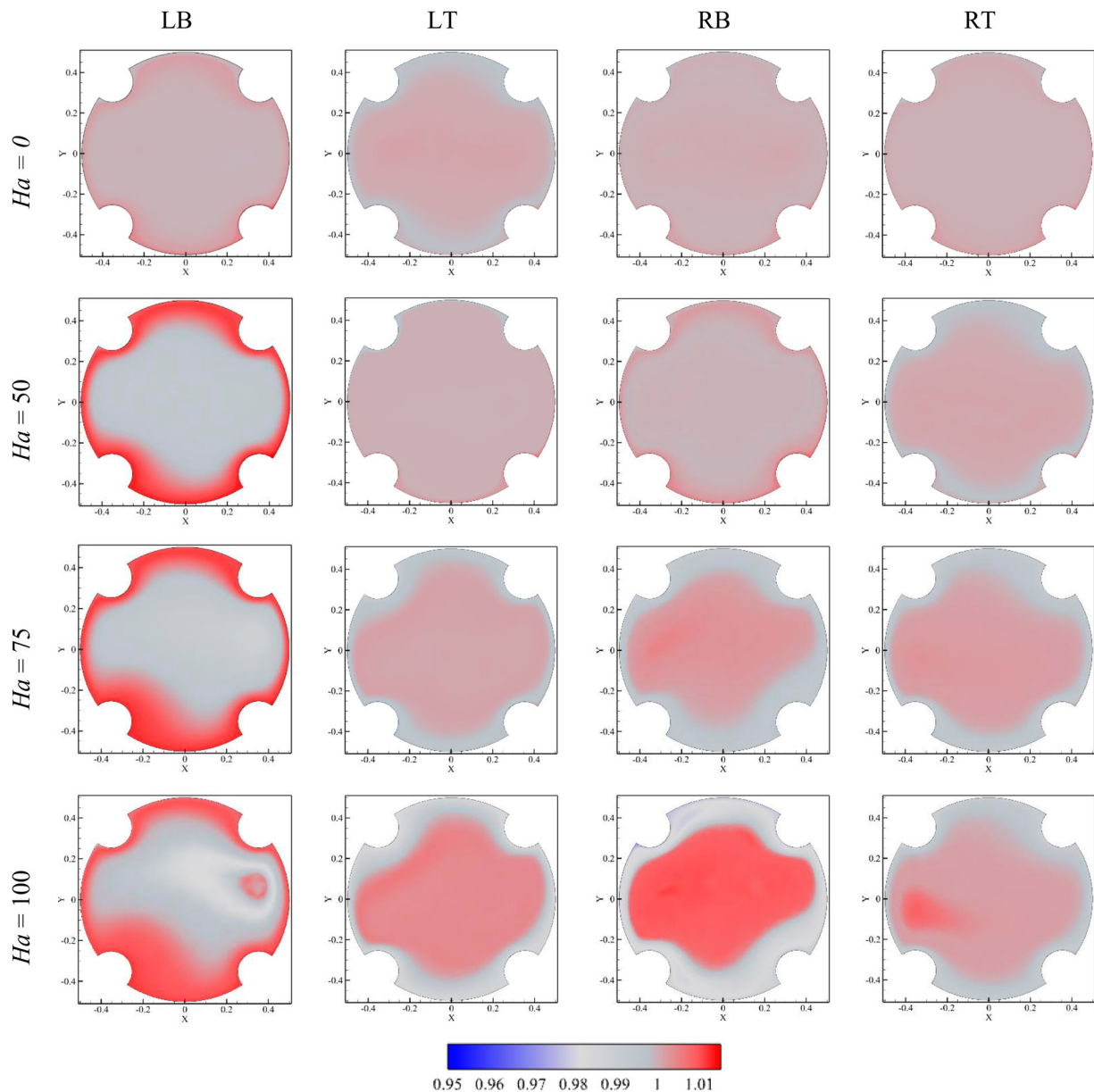


**Figure 7.** Nanoparticles concentration change on  $Ha$  and  $\delta$  when  $Ra = 5 \times 10^5$ ,  $\varphi = 5\%$ ,  $Pr = 7$ , and  $M_{nf} = 3 \times 10^4$ .



force has shifted the temperature line  $\theta = 0.25$  from left to the middle for LB case when  $M_{nf} = 1 \times 10^4$ . As seen, the change of isotherm patterns is mostly limited to the bottom left area of the enclosure where the magnetic source is located. Further increase of  $M_{nf}$ , impacts more temperature levels. For instance, the isotherms  $\theta = 0.35$  and  $\theta = 0.45$  have also been shifted towards the middle, and  $\theta = 0.25$  has been pushed to the right when  $M_{nf} = 4 \times 10^4$ . Placing the magnetic source at the top induces minor shifts in isotherms. However, when  $M_{nf}$  increases to  $4 \times 10^4$ , the local change of isotherms is obvious. For the case of LB, the increase of  $M_{nf}$  compacts the isotherms next to cold and hot walls leading to the rise of temperature gradients and consequently a better heat transfer rate (higher Nusselt number). The Kelvin force is a temperature-dependent body force that can contribute to the buoyancy force and boost the natural convection circulations or acts against it and weakens the free convection circulations, depending on the location of the magnetic source.

The dependency of streamlines on  $M_{nf}$  for different situations of magnetic source has shown in Figure 9. The results show that when  $M_{nf} = 0$ , the streamlines are still under the influence of magnetic source locations due to the presence of Lorentz forces ( $Ha = 50$ ). The streamlines create strong circulation patterns in an opposite location to the placement of the magnetic source. Indeed, the magnetic source locally suppresses the fluid flow next to its location due to the Lorentz force. However, the Kelvin force tends to boost the flow circulation by inducing a non-uniform local body force on the nanofluid. As seen, the distance between streamlines increases next to each magnetic source, indicating a reduction in the fluid velocity and circulation strength. Figure 10 illustrates the impact of  $M_{nf}$  on the nanoparticle concentration distributions. Interestingly, the LB case leads to the most uniform distribution of nanoparticles in the enclosure. The maximum change in nanoparticle concentration can be observed to be 1.01, which occurs in the RB case and at the

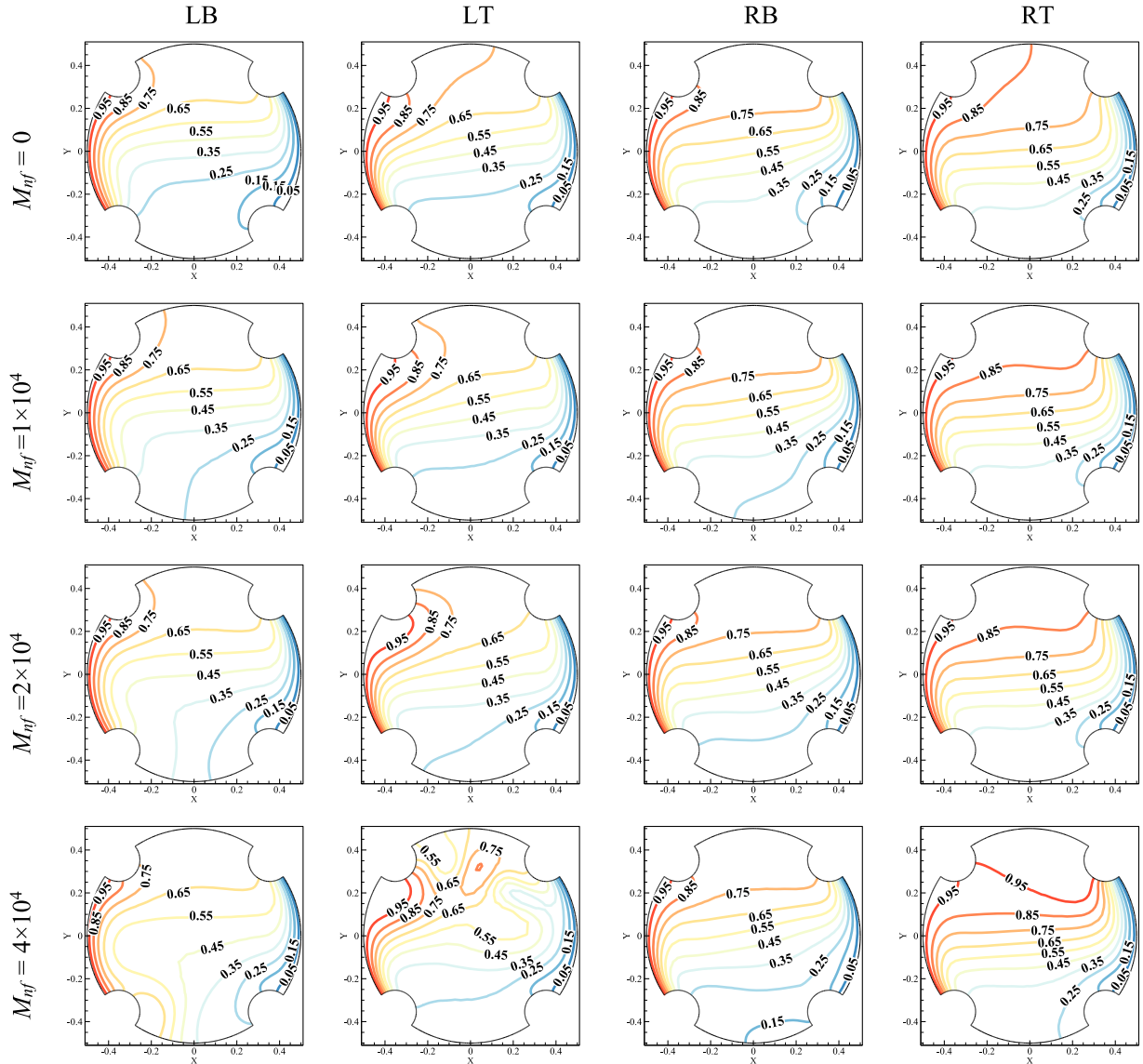


**Figure 8.** Isotherm lines change on  $M_{nf}$  and  $\delta$  when  $Ra = 5 \times 10^5$ ,  $\varphi = 5\%$ ,  $Pr = 7$ , and  $Ha = 50$ .



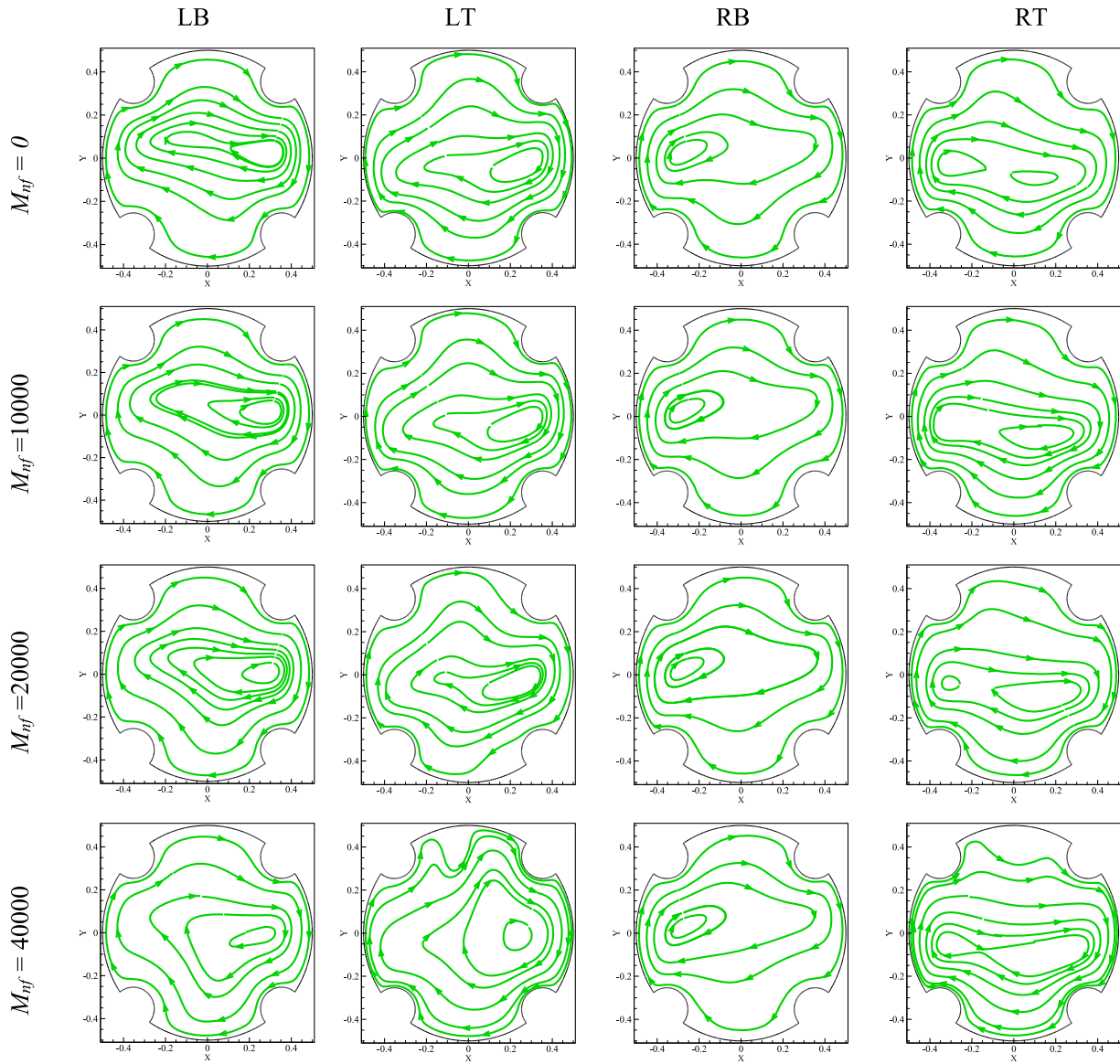


**Figure 9.** Streamlines change on  $M_{nf}$  and  $\delta$  when  $Ra = 5 \times 10^5$ ,  $\varphi = 5\%$ ,  $Pr = 7$ , and  $Ha = 50$ .

highest value of  $M_{nf}$ . The grey area shows the regions with a nanoparticle concentration below the average nanoparticle concentration  $\phi = 1$ .

Table 4 explores the relationship between the average Nusselt number ( $Nu_{avg}$ ) and the  $Ha$ , considering various positions of the magnetic source. Even when  $Ha$  is zero, the magnetic source's location significantly influences  $Nu_{avg}$  due to the effects of the Kelvin force. Indeed, when  $Ha = 0$ , the only force induced by the MF refers to the Kelvin force, which contributes to the reinforcement of the nanofluid movement. The highest recorded  $Nu_{avg}$ , standing at 4.92, is observed in the LB case when  $Ha$  is at zero. This is corroborated by the isotherms, which indicate that situating the magnetic source at the left bottom generates a pronounced temperature gradient at the hot and cold walls, thereby amplifying the rate of heat transfer. For a Hartmann number of zero, the order of cases from highest to lowest  $Nu_{avg}$  are as follows: RT, LT, and RB. The increase of Hartmann number boosts the resistive force against the

**Table 4.** Dependency of the  $Nu_{avg}$  on  $Ha$  for various locations of the magnetic source when  $M_{nf} = 30,000$ ,  $\varphi = 5\%$ ,  $Pr = 7$ , and  $Ra = 5 \times 10^5$ .

$Ha$	LB	LT	RB	RT
0	4.92	4.72	4.53	4.75
50	3.43	3.40	3.48	3.16
75	2.77	2.62	2.84	2.37
100	2.02	1.85	2.07	2.02

fluid movement and reduces the average Nusselt number due to the suppression of natural convection circulations. As  $Ha$  increases, it diminishes the favourable influence of  $M_{nf}$  on the average Nusselt number. For instance, at  $Ha = 100$ , the hierarchy of the average Nusselt number, from highest to lowest, was changed as follows: RB, LB and RT (which are equal), and finally, LT. As  $Ha$  increases from zero to 100,  $Nu_{Avg}$  decreases by approximately 60% for all cases.

Table 5 illustrates the relationship between the average Nusselt number and  $M_{nf}$  for various locations of

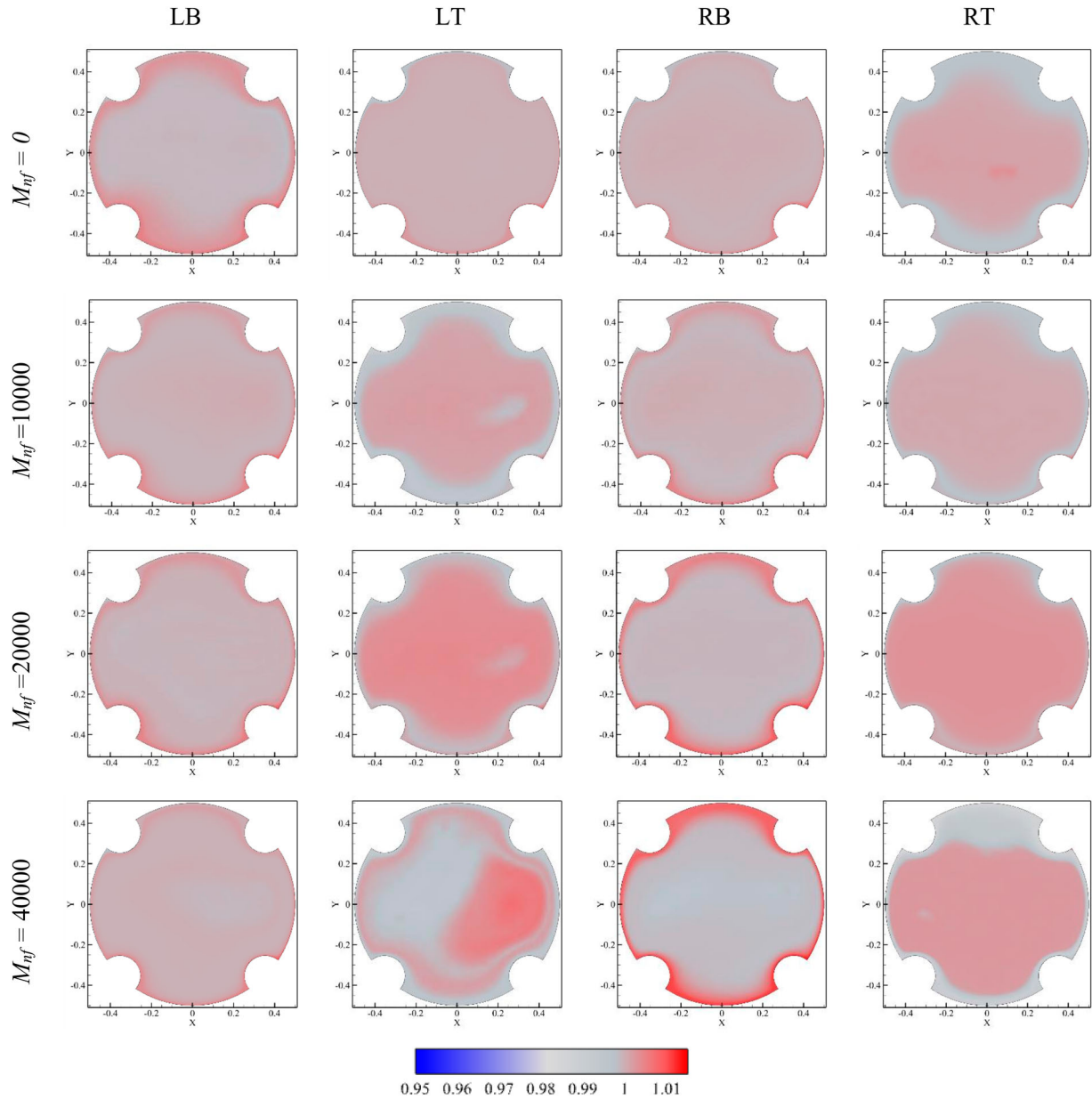


**Figure 10.** Nanoparticles concentration change on  $M_{nf}$  and  $\delta$  when  $Ra = 5 \times 10^5$ ,  $\varphi = 5\%$ ,  $Pr = 7$ , and  $Ha = 50$ .

magnetic sources. LB, LT, RB, and RT represent the four corners of the enclosure where the magnetic source can be placed. Since the Kelvin force induces a temperature-dependent body force, it can boost or deteriorate the natural convection flows.  $Nu_{avg}$  values range from 3.46 at the LT to 3.17 at RT when  $M_{nf} = 0$  (indicating no Kelvin force). This suggests that placing the magnetic source at the upper left corner leads to a better heat transfer when only Lorentz force is available ( $Ha = 50$ ). As  $M_{nf}$  increases from 0 to  $4 \times 10^4$ ,  $Nu_{avg}$  increases from 3.31 to 3.53 on the left (LB) and from 3.40 to 3.84 on the right (RB). Thus, for RB case, the Kelvin force improved the average Nusselt number by 11.5% when  $M_{nf}$  increases from zero to its maximum value. Similarly, it is estimated that  $Nu_{avg}$  has increased by 6.2% for the LB case. Thus, the increase of  $M_{nf}$  is favourable when the magnetic source is placed at the bottom.

**Table 5.** Dependency of the  $Nu_{avg}$  on  $M_{nf}$  for various displacements of the magnetic source when  $Ha = 50$ ,  $\varphi = 5\%$ ,  $Pr = 7$ , and  $Ra = 5 \times 10^5$ .

$M_{nf}$	LB (left bottom)	LT (left top)	RB (right bottom)	RT (right top)
0	3.31	3.46	3.40	3.17
100,000	3.343	3.31	3.55	3.06
200,000	3.429	2.99	3.68	2.89
400,000	3.53	2.66	3.84	2.79

On the contrary,  $Nu_{avg}$  decreases with increasing  $M_{nf}$  at the apex (both left and right). As  $M_{nf}$  increases from 0 to  $4 \times 10^4$ , the  $Nu_{avg}$  falls from 3.46 to 2.66 for LT and from 3.17 to 2.79 for RT. Thus, the increase of  $M_{nf}$  reduced the average Nusselt number by 23.1% and 12% for LT and RT cases, respectively. Therefore, the placement location of the magnetic source is a crucial design parameter that can enhance or deteriorates the convection heat transfer rate.

## 5. Conclusion

The present study addresses Lorentz and Kelvin's forces and their effect on the convection heat transfer and flow of a non-homogeneous nanofluid. A point source MF could be placed at four locations around the enclosure. Modelling of a non-homogeneous nanofluid was applied to consider the influence of particle migration and buoyancy forces due to the mass transfer effects. The finite element method was applied to solve the coupled governing equations. The nanoparticle distribution, isotherms, and streamlines were plotted. Besides, the heat transfer rate was characterized by the average Nusselt number and reported in tables. The results showed that the Kelvin force could influence the streamlines even in the absence of the Lorentz effects. The principal conclusions drawn from the research are as follows:

- The strategic location of the magnetic source plays a pivotal role in influencing the heat transfer rate (Nuavg). The research found that when the magnetic source is positioned at the bottom (both left and right), it enhances Nuavg as the magnetic field number (Mnf) escalates. Conversely, placing the magnetic source at the top leads to a decrease in Nuavg as Mnf grows. This observation underscores the importance of the magnetic source's location as a critical design parameter, as it can induce body forces that either assist or undermine the buoyancy forces. A decline in heat transfer rates was noted, attributable to the Lorentz force diminishing the flow circulations.
- When the magnetic source is situated at the bottom right of the enclosure, a maximum Kelvin force results in a Nuavg of 3.84. In contrast, without the presence of the Kelvin force, the Nuavg dips to 3.40. This finding suggests that the Kelvin force can enhance the average Nusselt number by 11.5%.
- An interesting outcome of the study is that the heat transfer rate can be reduced by 23.1% by positioning the magnetic source at the left top (LT). This finding provides crucial insights for design considerations in heat transfer systems.

## Disclosure statement

No potential conflict of interest was reported by the author(s).

## Funding

This study is supported via funding from Prince Sattam bin Abdulaziz University project number (PSAU/2023/R/1444). The study of Mikhail Sheremet and Mohammad Ghalambaz was supported by the Tomsk State University Development Programme (Priority-2030).

## Data availability statement

All data has been reported in the paper.

## ORCID

Mohammad Ghalambaz  <http://orcid.org/0000-0003-0965-2358>

## References

- [1] Ma Y, Mohebbi R, Rashidi MM, et al. Numerical study of MHD nanofluid natural convection in a baffled U-shaped enclosure. *Int J Heat Mass Transf.* 2019;130:123–134. doi:10.1016/j.ijheatmasstransfer.2018.10.072.
- [2] Bondarenko DS, Sheremet MA, Oztop HF, et al. Natural convection of Al<sub>2</sub>O<sub>3</sub>/H<sub>2</sub>O nanofluid in a cavity with a heat-generating element. Heatline visualization. *Int J Heat Mass Transf.* 2019;130:564–574. doi:10.1016/j.ijheatmasstransfer.2018.10.091.
- [3] Alsabery AI, Sheremet MA, Chamkha AJ, et al. Impact of nonhomogeneous nanofluid model on transient mixed convection in a double lid-driven wavy cavity involving solid circular cylinder. *Int J Mech Sci.* 2019;150:637–655. doi:10.1016/j.ijmecsci.2018.10.069.
- [4] Jalili B, Aghaee N, Jalili P, et al. Novel usage of the curved rectangular fin on the heat transfer of a double-pipe heat exchanger with a nanofluid. *Case Studies in Thermal Engineering.* 2022;35:102086. doi:10.1016/j.csite.2022.102086.
- [5] Jalili P, Kazerani K, Jalili B, et al. Investigation of thermal analysis and pressure drop in non-continuous helical baffle with different helix angles and hybrid nano-particles. *Case Studies in Thermal Engineering.* 2022;36:102209. doi:10.1016/j.csite.2022.102209.
- [6] Dinarvand S, Berrehal H, Pop I, et al. Blood-based hybrid nanofluid flow through converging/diverging channel with multiple slips effect: a development of Jeffery-Hamel problem. *Int J Numer Methods Heat Fluid Flow.* 2023;33(3):1144–1160. doi:10.1108/HFF-08-2022-0489.
- [7] Sheremet MA, Pop I, Rahman MM. Three-dimensional natural convection in a porous enclosure filled with a nanofluid using buongiorno's mathematical model. *Int J Heat Mass Transf.* 2015;82:396–405. doi:10.1016/j.ijheatmasstransfer.2014.11.066.
- [8] Ibrahim M, Berrouk AS, Saeed T, et al. Lattice Boltzmann-based numerical analysis of nanofluid natural convection in an inclined cavity subject to multiphysics fields. *Sci Rep.* 2022;12:1–8. doi:10.1038/s41598-021-99269-x.
- [9] Paroncini M, Corvaro F, Montucchiari A, et al. A numerical and experimental analysis on natural convective heat transfer in a square enclosure with partially active side walls. *Exp Therm Fluid Sci.* 2012;36:118–125. doi:10.1016/j.expthermflusci.2011.09.004.
- [10] Sheikholeslami M, Chamkha AJ. Flow and convective heat transfer of a ferro-nanofluid in a double-sided lid-driven cavity with a wavy wall in the presence of a variable magnetic field. *Numerical Heat Transfer, Part A: Applications.* 2016;69(10):1186–1200. doi:10.1080/10407782.2015.1125709.
- [11] Ghalambaz M, Sabour M, Sazgara S, et al. 2020, Insight into the dynamics of ferrohydrodynamic (FHD) and magnetohydrodynamic (MHD) nanofluids inside a hexagonal cavity in the presence of a non-uniform magnetic field. *J Magn Magn Mater.* 2020; 497:166024. doi:10.1016/j.jmmm.2019.166024.
- [12] Sami S. Impact of magnetic field on the enhancement of performance of thermal solar collectors using nanofluids. *Int J Ambient Energy.* 2019;40(8):875–884. doi:10.1080/01430750.2018.1437561.

- [13] Ali MM, Akhter R, Alim MA. MHD natural convection and entropy generation in a grooved enclosure filled with nanofluid using two-component non-homogeneous model. *SN Appl Sci.* 2020;2:1–11. doi:10.1007/s42452-019-1805-5.
- [14] Sathiyamoorthy M, Chamkha AJ. Natural convection flow under magnetic field in a square cavity for uniformly (or) linearly heated adjacent walls. *Int J Numer Methods Heat Fluid Flow.* 2012;22(5):677–698. doi:10.1108/09615531211231307.
- [15] Jalili B, Sadighi S, Jalili P, et al. Numerical analysis of MHD nanofluid flow and heat transfer in a circular porous medium containing a Cassini oval under the influence of the Lorentz and buoyancy forces. *Heat Transfer.* 2022;51(7):6122–6138. doi:10.1002/htj.22582.
- [16] Jalili B, Jalili P, Sadighi S, et al. Effect of magnetic and boundary parameters on flow characteristics analysis of micropolar ferrofluid through the shrinking sheet with effective thermal conductivity. *Chin J Phys.* 2021;71:136–150. doi:10.1016/j.cjph.2020.02.034.
- [17] Jalili P, Azar AA, Jalili B, et al. Heat transfer analysis in cylindrical polar system with magnetic field: A novel hybrid analytical and numerical technique. *Case Stud Therm Eng.* 2022;40:102524. doi:10.1016/j.csite.2022.102524.
- [18] Jalili B, Ganji AD, Jalili P, et al. Thermal analysis of Williamson fluid flow with Lorentz force on the stretching plate. *Case Studies in Thermal Engineering.* 2022;39:102374. doi:10.1016/j.csite.2022.102374.
- [19] Jalili P, Narimisa H, Jalili B, et al. A novel analytical approach to micro-polar nanofluid thermal analysis in the presence of thermophoresis, Brownian motion and Hall currents. *Soft Comput.* 2023;27(2):677–689. doi:10.1007/s00500-022-07643-2.
- [20] Dinarvand S, Rostami MN. Three-dimensional squeezed flow of aqueous magnetite–graphene oxide hybrid nanofluid: A novel hybridity model with analysis of shape factor effects. *Proc Inst Mech Eng Part E J Process Mech Eng.* 2020;234(2):193–205. doi:10.1177/0954408920906274.
- [21] Izady M, Dinarvand S, Pop I, et al. Flow of aqueous Fe<sub>2</sub>O<sub>3</sub>–CuO hybrid nanofluid over a permeable stretching/shrinking wedge: A development on Falkner–Skan problem. *Chin J Phys.* 2021;74:406–420. doi:10.1016/j.cjph.2021.10.018.
- [22] Berrehal H, Dinarvand S, Khan I. Mass-based hybrid nanofluid model for entropy generation analysis of flow upon a convectively-warmed moving wedge. *Chin J Phys.* 2022;77:2603–2616. doi:10.1016/j.cjph.2022.04.017.
- [23] Dinarvand S, Nejad AM. Off-centered stagnation point flow of an experimental-based hybrid nanofluid impinging to a spinning disk with low to high non-alignments. *Int J Numer Methods Heat Fluid Flow.* 2021;32(8):2799–2818.
- [24] Huang Y, Ma M, Xu M, et al. Numerical study of natural convective heat transfer of nanofluids within a porous corrugated triangular cavity in the presence of a magnetic field. *Numerical Heat Transfer, Part A: Applications.* 2022;82(11):716–742. doi:10.1080/10407782.2022.2083867.
- [25] Alsabery AI, Vaezi M, Tayebi T, et al. Nanofluid mixed convection inside wavy cavity with heat source: A non-homogeneous study. *Case Studies in Thermal Engineering.* 2022;34:102049. doi:10.1016/j.csite.2022.102049.
- [26] Mahesh A, Raju CSK, Babu MJ, et al. Entropy generation optimization in an unsteady hybrid nanofluid flow between two rotating disks: a numerical bioconvection model. *Waves Random Complex Media.* 2022: 1–32. doi:10.1080/17455030.2022.2142320.
- [27] Sannad M, Hussein AK, Abidi A, et al. Numerical study of MHD natural convection inside a cubical cavity loaded with copper-water nanofluid by using a nonhomogeneous dynamic mathematical model. *Mathematics.* 2022;10(12):2072. doi:10.3390/math10122072.
- [28] Liu Z, Yan Y, Fu R, et al. Enhancement of solar energy collection with magnetic nanofluids. *Therm Sci Eng Prog.* 2018;8:130–135. doi:10.1016/j.tsep.2018.08.015.
- [29] Gan Jia Gui N, Stanley C, Nguyen NT, et al. Ferrofluids for heat transfer enhancement under an external magnetic field. *Int J Heat Mass Transf.* 2018;123:110–121. doi:10.1016/j.ijheatmasstransfer.2018.02.100.
- [30] Ren J, Jin Z, Huang X, et al. A lattice Boltzmann method for two-phase nanofluid under variable non-uniform magnetic fields. *J Appl Phys.* 2022;132(17):174703.
- [31] Ashorynejad HR, Shahriari A. MHD natural convection of hybrid nanofluid in an open wavy cavity. *Results Phys.* 2018;9:440–455.
- [32] Szabo PSB, Früh W-G. The transition from natural convection to thermomagnetic convection of a magnetic fluid in a non-uniform magnetic field. *J Magn Magn Mater.* 2018;447:116–123. doi:10.1016/j.jmmm.2017.09.028.
- [33] Javed T, Siddiqui MA. Effect of MHD on heat transfer through ferrofluid inside a square cavity containing obstacle/heat source. *Int J Therm Sci.* 2018;125:419–427. doi:10.1016/j.ijthermalsci.2017.12.009.
- [34] Bahiraei M, Hangi M, Rahbari A. A two-phase simulation of convective heat transfer characteristics of water–Fe<sub>3</sub>O<sub>4</sub> ferrofluid in a square channel under the effect of permanent magnet. *Appl Therm Eng.* 2019;147:991–997. doi:10.1016/j.applthermaleng.2018.11.011.
- [35] Mohammadpourfard M, Aminfar H, Ahangar Zonouzi S. Numerical investigation of the magnetic field effects on the entropy generation and heat transfer in a nanofluid filled cavity with natural convection. *Heat Transf-Asian Res.* 2017;46(5):409–433. doi:10.1002/htj.21222.
- [36] Abdi H, Motlagh SY, Soltanipour H. Numerical study of two-phase flow in a square cavity under magnetic field of parallel wires. *Meccanica.* 2021;56(8):2005–2020. doi:10.1007/s11012-021-01347-x.
- [37] Sheikholeslami M, Bhatti MM. Forced convection of nanofluid in presence of constant magnetic field considering shape effects of nanoparticles. *Int J Heat Mass Transf.* 2017;111:1039–1049. doi:10.1016/j.ijheatmasstransfer.2017.04.070.
- [38] Biswas N, Mondal MK, Mandal DK, et al. A narrative loom of hybrid nanofluid-filled wavy walled tilted porous enclosure imposing a partially active magnetic field. *Int J Mech Sci.* 2022;217:107028. doi:10.1016/j.ijmecsci.2021.107028.
- [39] Mondal MK, Biswas N, Datta A, et al. Magneto-hydro thermal convective dynamics of hybrid nanofluid-packed partially cooled porous cavity: effect of half-sinusoidal heating. *J Therm Anal Calorim.* 2023;148(9):3903–3928. doi:10.1007/s10973-023-11959-y.
- [40] Biswas N, Mandal DK, Manna NK, et al. Enhanced energy and mass transport dynamics in a thermo-magneto-bioconvective porous system containing oxytactic bacteria and nanoparticles: cleaner energy application. *Energy.* 2023;263:125775. doi:10.1016/j.energy.2022.125775.
- [41] Chatterjee D, Biswas N, Manna NK, et al. Effect of discrete heating-cooling on magneto-thermal-hybrid



- nanofluidic convection in cylindrical system. *Int J Mech Sci.* **2023**;238:107852. doi:[10.1016/j.ijmecsci.2022.107852](https://doi.org/10.1016/j.ijmecsci.2022.107852).
- [42] Chatterjee D, Biswas N, Manna NK, et al. Magneto-nanofluid flow in cylinder-embedded discretely heated-cooled annular thermal systems: conjugate heat transfer and thermodynamic irreversibility. *J Magn Magn Mater.* **2023**;569:170442. doi:[10.1016/j.jmmm.2023.170442](https://doi.org/10.1016/j.jmmm.2023.170442).
- [43] Saha A, Manna NK, Ghosh K, et al. Analysis of geometrical shape impact on thermal management of practical fluids using square and circular cavities. *The European Physical Journal Special Topics.* **2022**;231(13–14):2509–2537. doi:[10.1140/epjs/s11734-022-00593-8](https://doi.org/10.1140/epjs/s11734-022-00593-8).
- [44] Amani M, Amani P, Bahiraei M, et al. Latest developments in nanofluid flow and heat transfer between parallel surfaces: A critical review. *Adv Colloid Interface Sci.* **2021**;294:102450. doi:[10.1016/j.cis.2021.102450](https://doi.org/10.1016/j.cis.2021.102450).
- [45] Garoosi F, Bagheri G, Rashidi MM. Two phase simulation of natural convection and mixed convection of the nanofluid in a square cavity. *Powder Technol.* **2015**;275:239–256. doi:[10.1016/j.powtec.2015.02.013](https://doi.org/10.1016/j.powtec.2015.02.013).
- [46] Godson L, Raja B, Mohan Lal D, et al. Enhancement of heat transfer using nanofluids – an overview. *Renewable Sustainable Energy Rev.* **2010**;14(2):629–641. doi:[10.1016/j.rser.2009.10.004](https://doi.org/10.1016/j.rser.2009.10.004).
- [47] Sheremet MA, Pop I. Conjugate natural convection in a square porous cavity filled by a nanofluid using Buongiorno's mathematical model. *Int J Heat Mass Transf.* **2014**;79:137–145. doi:[10.1016/j.ijheatmasstransfer.2014.07.092](https://doi.org/10.1016/j.ijheatmasstransfer.2014.07.092).
- [48] Soltanipour H. Numerical analysis of two-phase ferrofluid forced convection in an annulus subjected to magnetic sources. *Appl Therm Eng.* **2021**;196:117278. doi:[10.1016/j.applthermaleng.2021.117278](https://doi.org/10.1016/j.applthermaleng.2021.117278).
- [49] Dawar A, Wakif A, Thumma T, et al. Towards a new MHD non-homogeneous convective nanofluid flow model for simulating a rotating inclined thin layer of sodium alginate-based iron oxide exposed to incident solar energy. *Int Commun Heat Mass Transfer.* **2022**;130:105800. doi:[10.1016/j.icheatmasstransfer.2021.105800](https://doi.org/10.1016/j.icheatmasstransfer.2021.105800).
- [50] Sheikholeslami M, Ganji D. Ferrofluid convective heat transfer under the influence of external magnetic source. *Alexandria Eng J.* **2018**;57(1):49–60. doi:[10.1016/j.aej.2016.11.007](https://doi.org/10.1016/j.aej.2016.11.007).
- [51] Buongiorno J. Convective transport in nanofluids. *J Heat Transfer ASME.* **2006**;128:240–250. doi:[10.1115/1.2150834](https://doi.org/10.1115/1.2150834).
- [52] Ghalambaz M, Zadeh SMH, Mehryan S, et al. Non-Newtonian behavior of an electrical and magnetizable phase change material in a filled enclosure in the presence of a non-uniform magnetic field. *Int Commun Heat Mass Transfer.* **2020**;110:104437. doi:[10.1016/j.icheatmasstransfer.2019.104437](https://doi.org/10.1016/j.icheatmasstransfer.2019.104437).
- [53] Ghalambaz M, Hashem Zadeh SM, Mehryan SAM, et al. Analysis of melting behavior of PCMs in a cavity subject to a non-uniform magnetic field using a moving grid technique. *Appl Math Model.* **2020**;77:1936–1953. doi:[10.1016/j.apm.2019.09.015](https://doi.org/10.1016/j.apm.2019.09.015).
- [54] Mehryan SAM, Tahmasebi A, Izadi M, et al. Melting behavior of phase change materials in the presence of a non-uniform magnetic-field due to two variable magnetic sources. *Int J Heat Mass Transf.* **2020**;149:119184. doi:[10.1016/j.ijheatmasstransfer.2019.119184](https://doi.org/10.1016/j.ijheatmasstransfer.2019.119184).
- [55] Sheikholeslami M, Vajravelu K. Nanofluid flow and heat transfer in a cavity with variable magnetic field. *Appl Math Comput.* **2017**;298:272–282. doi:[10.1016/j.amc.2016.11.025](https://doi.org/10.1016/j.amc.2016.11.025).
- [56] Sheikholeslami M, Hayat T, Alsaedi A. Numerical study for external magnetic source influence on water based nanofluid convective heat transfer. *Int J Heat Mass Transf.* **2017**;106:745–755. doi:[10.1016/j.ijheatmasstransfer.2016.09.077](https://doi.org/10.1016/j.ijheatmasstransfer.2016.09.077).
- [57] Reddy JN. Introduction to the finite element method. New York: McGraw-Hill Education; **2019**.
- [58] Löhner R. Applied computational fluid dynamics techniques: an introduction based on finite element methods. 2nd ed. Hoboken: John Wiley & Sons; **2008**.
- [59] Zienkiewicz OC, Taylor RL, Nithiarasu P. The finite element method for fluid dynamics. 7th ed. Oxford: Butterworth-Heinemann; **2014**.
- [60] Connor J, Brebbia CA. Finite element techniques for fluid flow. London: Newnes; **2013**.
- [61] Pepper D. The intermediate finite element method: fluid flow and heat transfer applications. New York: Routledge; **2017**.
- [62] Biswas N, Mondal MK, Manna NK, et al. Implementation of partial magnetic fields to magneto-thermal convective systems operated using hybrid-nanoliquid and porous media. *Proc Inst Mech Eng Part C J Mech Eng Sci.* **2022**;236(10):5687–5704. doi:[10.1177/09544062211060168](https://doi.org/10.1177/09544062211060168).
- [63] Manna NK, Mondal MK, Biswas N. A novel multi-banding application of magnetic field to convective transport system filled with porous medium and hybrid nanofluid. *Phys Scr.* **2021**;96(6):065001. doi:[10.1088/1402-4896/abecbf](https://doi.org/10.1088/1402-4896/abecbf).
- [64] Dutta S, Pati S, Baranyi L. Numerical analysis of magnetohydrodynamic natural convection in a nanofluid filled quadrantal enclosure. *Case Studies in Thermal Engineering.* **2021**;28:101507. doi:[10.1016/j.csite.2021.101507](https://doi.org/10.1016/j.csite.2021.101507).
- [65] Sajjadi H, Delouei AA, Sheikholeslami M, et al. Simulation of three dimensional MHD natural convection using double MRT Lattice Boltzmann method. *Physica A.* **2019**;515:474–496. doi:[10.1016/j.physa.2018.09.164](https://doi.org/10.1016/j.physa.2018.09.164).
- [66] Manna NK, Biswas N. Magnetic force vectors as a new visualization tool for magnetohydrodynamic convection. *Int J Therm Sci.* **2021**;167:107004. doi:[10.1016/j.ijthermalsci.2021.107004](https://doi.org/10.1016/j.ijthermalsci.2021.107004).